

The substrate-induced reduction of graphene thermal conductivity

S. V. Koniakhin,^{1,2,*} O. I. Utesov,^{3,†} I. N. Terterov,¹ and A. V. Nalitov⁴

¹*St. Petersburg Academic University, Khlopina 8/3, 194021 St. Petersburg, Russia*

²*Ioffe Physical-Technical Institute of the Russian Academy of Sciences, 194021 St. Petersburg, Russia*

³*Petersburg Nuclear Physics Institute NRC "Kurchatov Institute", Gatchina, St. Petersburg 188300, Russia*

⁴*School of Physics and Astronomy, University of Southampton, Southampton SO17 1BJ, United Kingdom*

We develop the theory of heat conductivity in supported graphene, accounting for coherent phonon scattering on disorder induced by an amorphous substrate. We derive spectra for in-plane and out-of-plane phonons in the framework of Green's function approach. The energetic parameters of the theory are obtained using the molecular dynamics simulations for graphene on SiO₂ substrate. The heat conductivity is calculated within the Boltzmann transport equation. We find that the interaction with the substrate drastically reduces the phonon lifetime and completely suppresses the contribution of ZA phonons to the heat conductivity. As result, the total heat conductivity is reduced by several times, which lies in agreement with the current experimental data. The considered effect is important for managing thermal properties of the graphene based electronic devices.

I. INTRODUCTION

Due to its outstanding properties, graphene, a honeycomb monolayer of carbon atoms, attracts great attention as a material for application in the future nanoscale electronics. The mechanical^{1,2}, electronic³⁻⁵ properties of graphene, various radiation driven effects⁶⁻⁸ and thermoelectric⁹ phenomena in graphene are among the hottest topics of recent studies in condensed matter physics.

Along with other carbon-based materials, graphene reveals extremely high thermal conductivity κ . The room temperature thermal conductivity of suspended graphene reaches $5000 \text{ W m}^{-1} \text{ K}^{-1}$ ^{10,11}. For application of graphene as a component of electronic devices and controlling the carrier density it is commonly gated. This requires close contact between graphene sheet and dielectric substrate like SiO₂. Electron scattering on the surface charged impurities^{5,12}, surface corrugations¹³⁻¹⁵, atomic steps¹⁶ and surface polar phonons¹⁷⁻¹⁹ reduces electric conductivity of graphene. The same effect is expected for heat conductivity. Accounting for graphene layers and conductive traces as heat sinks requires a quantitative estimate of this effect. Also the estimations of acoustic phonon lifetime and mean free path are obligate for calculating phonon drag contributions to thermopower in graphene^{20,21}.

Previously the effect of substrate on thermal properties of graphene was investigated experimentally, from theoretical standpoint and by molecular dynamics simulations. The experimental studies of heat conductivity in suspended graphene are based on the Raman optothermal method²²⁻²⁷, and reveal values above $2000 \text{ W m}^{-1} \text{ K}^{-1}$. Investigation of the supported graphene thermal properties is based on the electrical heating and give several times lower values of thermal conductivity²⁸. Other works, where the supported graphene is studied, focus mainly on graphene electrical properties with heat conductivity being a secondary result^{29,30}. The table in Ref.¹¹ summarizes current studies on graphene thermal

conductivity.

The heat conductivity is governed by the phonon dispersion and relaxation process^{10,11}. The theoretically investigated mechanisms of phonon relaxation include boundary scattering, point defect scattering and anharmonic processes³¹⁻³⁵. The effect of the substrate is out of consideration in most current theoretical works. In the supplementary online materials of Ref.²⁸, the spot contact model within Fermi golden rule formalism developing the Klemens approach³⁶ for phonon scattering, was employed for accounting for a substrate. However, the case of randomly distributed defects with close to atomic concentration needs a theory based on Green's function to account for coherent scattering.

The molecular dynamics (MD) is also used for investigating thermal conductivity of graphene³⁷⁻⁴⁰ and carbon nanotubes^{41,42}. Such studies include modeling of phonon of graphene on amorphous substrate. Ref.⁴³ is devoted to molecular dynamics simulations of graphene on SiO₂ substrate and show that van der Waals interaction reduces relaxation time of intrinsic acoustic phonons in graphene. The non-equilibrium MD simulation demonstrates reduction of thermal transport in graphene on SiO₂⁴⁴. Although MD simulation is a promising and powerful tool for investigating vibrational properties of solids, it is necessary to compare the obtained results with independent analytical approach.

Here we address the effect of amorphous substrate on the phonon dispersion and lifetimes in graphene within the Green's function formalism⁴⁵. The parameters of the perturbing substrate-induced van der Waals potential required by the developed analytical theory were obtained with MD simulations. In-plane (LA,TA) and flexural (ZA) phonons were considered and corresponding contributions to heat conductivity were obtained within the BTE approach.

The rest of the paper is organized as follows. In the beginning of Section II A we introduce the general form of graphene Hamiltonian accounting for interaction with the substrate. In the next two subsections we derive spectra for the in-plane (II B) and flexural (II C) phonons

within the perturbation theory approach. In Subsection IID we calculate the contributions of various phonon scattering mechanisms to heat conductivity using the Boltzmann transport equation (BTE). In Subsection IIE we describe the MD simulation, performed to estimate energetic parameters, required by the developed perturbation theory. Section III aggregates results for spectra and lifetimes for in-plane (Subsection III A) and ZA (Subsection III B) phonons and results for heat conductivity of supported graphene in Subsection III C.

II. THEORY

A. Perturbations to conventional graphene Hamiltonian due to the substrate

We start with considering static properties of graphene on the substrate. Due to the interplay between carbon-carbon and carbon-substrate forces carbon atoms in graphene layer are shifted from their regular positions. These static substrate-induced displacements are described by the vector set $(\mathbf{r}_{i0}, z_{i0})$, where the i index spans all sites, \mathbf{r}_{i0} and z_{i0} are in-plane and out of plane displacements correspondingly. Thus, we write the following equation for the graphene potential energy

$$E = \sum_i \left(U_{sub}(\mathbf{r}_{i0}, z_{i0}) + \sum_j \frac{K(\delta R_{ij})^2}{2} \right), \quad (1)$$

where U_{sub} is the potential energy stemming from the interaction with the substrate. After simple calculations we get

$$E = \sum_i \left(U_{sub}(\mathbf{r}_{i0}, z_{i0}) + \sum_j \frac{K}{2} [(\mathbf{e}_{ij}(\mathbf{r}_{i0} - \mathbf{r}_{j0}))^2 + \frac{((z_{i0} - z_{j0})^2 + (r_{i0}^\tau - r_{j0}^\tau)^2)^2}{4R^2}] \right). \quad (2)$$

Here r^τ is a perpendicular to bond in-plane displacement, explicitly $r_{i0}^\tau - r_{j0}^\tau = |(\mathbf{r}_{i0} - \mathbf{r}_{j0}) - (\mathbf{e}_{ij} \cdot (\mathbf{r}_{i0} - \mathbf{r}_{j0}))\mathbf{e}_{ij}|$. Positions of carbon atoms on the amorphous substrate satisfy standard equations for classical energy minimum ($\partial E / \partial \mathbf{R}_i = 0$). Introducing small deviations x_i, y_i, z_i from equilibrium positions we get a perturbation of the conventional in-plane phonon Hamiltonian:

$$\delta H_{in-plane} = \sum_i \left[\frac{1}{2} \frac{\partial^2 U_{sub}}{\partial x^2}(\mathbf{r}_{i0}, z_{i0}) x_i^2 + \frac{1}{2} \frac{\partial^2 U_{sub}}{\partial y^2}(\mathbf{r}_{i0}, z_{i0}) y_i^2 + \sum_j \frac{K(r_i^\tau - r_j^\tau)^2}{4R^2} (3(r_{i0}^\tau - r_{j0}^\tau)^2 + (z_{i0} - z_{j0})^2) \right]. \quad (3)$$

Also we get the following perturbation for ZA phonons:

$$\delta H_{ZA} = \sum_i \left[\frac{1}{2} \frac{\partial^2 U_{sub}}{\partial z^2}(\mathbf{r}_{i0}, z_{i0}) z_i^2 + \sum_j \frac{K(z_i - z_j)^2}{4R^2} (3(z_{i0} - z_{j0})^2 + (r_{i0}^\tau - r_{j0}^\tau)^2) \right], \quad (4)$$

The MD simulation described below shows that here the terms with z_{i0} are much larger than ones with r_{i0}^τ . An extra difference in prefactor 3 allows to omit the terms with r_{i0}^τ here, which is reflected in the definition of parameters β_{ij} in the beginning of section II C.

B. Theory for LA and TA phonons

The perturbation Hamiltonian for the in-plane phonons has the following form (cf. Eq. (3)):

$$\mathcal{V} = \sum_j \left[\frac{\gamma_j r_j^2}{2} + \sum_l \frac{\xi_{jl}(r_j^\tau - r_l^\tau)^2}{2} \right]. \quad (5)$$

Parameters γ_j and ξ_{jl} were determined using MD simulations. Let

$$\gamma = \left\langle \frac{\partial^2 U_{sub}}{\partial x^2}(\mathbf{r}_{i0}, z_{i0}) + \frac{\partial^2 U_{sub}}{\partial y^2}(\mathbf{r}_{i0}, z_{i0}) \right\rangle, \quad (6)$$

$$\tilde{\gamma}_i = \gamma_i - \gamma, \quad (7)$$

$$\xi = \left\langle \frac{K(3(r_{i0}^\tau - r_{j0}^\tau)^2 + (z_{i0} - z_{j0})^2)}{4R^2} \right\rangle, \quad (8)$$

$$\tilde{\xi}_{jl} = \xi_{jl} - \xi, \quad (9)$$

where angle brackets denote the averaging over disorder configurations. Obviously $\langle \tilde{\gamma}_i \rangle, \langle \tilde{\xi}_{il} \rangle = 0$. So we can divide perturbation (5) in two parts:

$$\mathcal{V} = \mathcal{V}_1 + \mathcal{V}_2, \quad (10)$$

$$\mathcal{V}_1 = \gamma \sum_j \left[\frac{r_j^2}{2} + \xi \sum_l \frac{(r_j^\tau - r_l^\tau)^2}{2} \right], \quad (11)$$

$$\mathcal{V}_2 = \sum_j \left[\frac{\tilde{\gamma}_j r_j^2}{2} + \sum_l \frac{\tilde{\xi}_{jl}(r_j^\tau - r_l^\tau)^2}{2} \right]. \quad (12)$$

It is easy to include \mathcal{V}_1 to the exact phonon spectrum, because it only shifts system vibrational eigenvalues (ω^2) by γ and slightly renormalizes sound speed c . One can see that the term with ξ in \mathcal{V}_1 contains additional factor $(\mathbf{e}_k - (\mathbf{e}_k \cdot \mathbf{e}_\nu)\mathbf{e}_\nu)^2$, where $\nu = 1, 2, 3$ indicates the bond index and phonon wave vector direction $\mathbf{e}_k = \frac{\mathbf{k}}{k}$. At small momenta k its average over momentum angle is almost 1/4, with negligible trigonal warping. Thus, in Debye model bare phonon spectrum reads:

$$\omega_k = \sqrt{\frac{\gamma}{m} + \left(1 + \frac{\xi}{2K}\right) c^2 k^2}. \quad (13)$$

From this expression one can see that the bare spectrum is gapped. Let \tilde{c} be the renormalized sound speed,

$$\tilde{c} = c \sqrt{\left(1 + \frac{\xi}{2K}\right)}. \quad (14)$$

We use the conventional quantized atom displacement representation:

$$r_j(\mathbf{R}_j, t) = \frac{1}{\sqrt{2mN}} \sum_k \frac{\mathbf{e}_k}{\sqrt{\omega_k}} (b_k e^{i\mathbf{k}\mathbf{R}_j} + b_k^\dagger e^{-i\mathbf{k}\mathbf{R}_j}), \quad (15)$$

where N is the number of unit cells in the system, b_k and b_k^\dagger are bosonic operators. Using this equation it is easy to show that

$$\mathcal{H}_0 = \sum_k \omega_k \left(b_k^\dagger b_k + \frac{1}{2} \right), \quad (16)$$

as in the case of standard gapless acoustic phonons. Using Eq.(15) we have the first part of perturbation (12) in the following form:

$$\begin{aligned} \mathcal{V}_2 &= \frac{1}{4mN} \sum_j \sum_{k_1, k_2} \frac{\mathbf{e}_{k_1} \cdot \mathbf{e}_{k_2} \tilde{\gamma}_j}{\sqrt{\omega_{k_1} \omega_{k_2}}} \\ &\times \left(b_{k_1} b_{k_2} e^{i(\mathbf{k}_1 + \mathbf{k}_2)\mathbf{R}_j} + b_{k_1}^\dagger b_{k_2} e^{i(\mathbf{k}_2 - \mathbf{k}_1)\mathbf{R}_j} \right) + H.C., \end{aligned} \quad (17)$$

where ‘‘H.C.’’ is for Hermitian conjugate. Simple estimation shows that main impact to phonon spectrum stems from normal terms in the perturbation and anomalous terms can be omitted. So including the second part of perturbation (12) yields:

$$\begin{aligned} \mathcal{V}_2 &= \frac{1}{2mN} \sum_j \sum_{k_1, k_2} \frac{b_{k_1}^\dagger b_{k_2} e^{i(\mathbf{k}_2 - \mathbf{k}_1)\mathbf{R}_j}}{\sqrt{\omega_{k_1} \omega_{k_2}}} \left[\tilde{\gamma}_j (\mathbf{e}_{k_1} \cdot \mathbf{e}_{k_2}) \right. \\ &+ \sum_l \left[\tilde{\xi}_{jl} (\mathbf{e}_{k_1} - (\mathbf{e}_{k_1} \cdot \mathbf{e}_{jl}) \mathbf{e}_{jl}) \cdot (\mathbf{e}_{k_2} - (\mathbf{e}_{k_2} \cdot \mathbf{e}_{jl}) \mathbf{e}_{jl}) \right. \\ &\left. \left. \times \left(1 - e^{-i\mathbf{k}_1(\mathbf{R}_l - \mathbf{R}_j)} \right) \left(1 - e^{i\mathbf{k}_2(\mathbf{R}_l - \mathbf{R}_j)} \right) \right] \right]. \end{aligned} \quad (18)$$

In the following calculations we use this definition for phonon Green’s function:

$$D_0(\omega, \mathbf{k}) = \frac{2\omega_k}{\omega^2 - \omega_k^2 + i0}. \quad (19)$$

First order in disorder strength correction to phonon self-energy part is given by the following equation (see Fig.1(b)):

$$\begin{aligned} \Sigma^{(1)}(\omega, \mathbf{k}) &= \frac{1}{2m\omega_k} \left[\frac{1}{N} \sum_j \left(\tilde{\gamma}_j \right. \right. \\ &+ \left. \left. \sum_l 2\tilde{\xi}_{jl} (1 - \cos \mathbf{k} \cdot \mathbf{e}_{jl}) (\mathbf{e}_k - (\mathbf{e}_k \cdot \mathbf{e}_{jl}) \mathbf{e}_{jl})^2 \right) \right] = 0, \end{aligned} \quad (20)$$

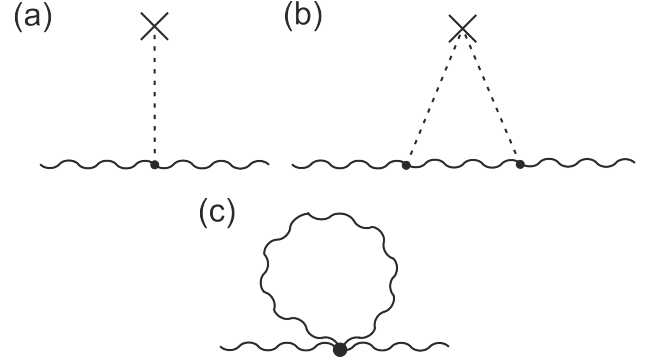


FIG. 1. Diagrams giving corrections to the phonon spectrum. a) - first order in $\tilde{\gamma}_i$ correction, which gives zero because $\langle \tilde{\gamma}_i \rangle = 0$, b) - second order correction, which is nonzero when the scattering is taking place on the same defect. Waved line is for phonons Green’s function and dashed line is for perturbing potential. c) Correction to ZA phonon spectrum due to phonon-phonon interaction.

because expression in the brackets contains $\langle \tilde{\gamma}_i \rangle$ and $\langle \tilde{\xi}_{jl} \rangle$, which are zero. Second order correction is given by the diagram shown in Fig.1(b). Let us first consider only the term with $\tilde{\gamma}_i$, as the other terms are negligible at small momenta and have no divergences. The corresponding equation reads:

$$\begin{aligned} \Sigma^{(2)}(\omega, \mathbf{k}) &= \frac{1}{4m^2 N^2 \omega_k} \\ &\times \sum_{j,l} \tilde{\gamma}_j \tilde{\gamma}_l \sum_q \frac{(\mathbf{e}_k \mathbf{e}_q)^2 D_0(\omega, \mathbf{k})}{\omega_q} e^{i(\mathbf{k} - \mathbf{q})(\mathbf{R}_j - \mathbf{R}_l)}. \end{aligned} \quad (21)$$

After averaging over disorder one gets:

$$\Sigma^{(2)}(\omega, \mathbf{k}) = \frac{\langle \tilde{\gamma}_i^2 \rangle v_0}{2m^2 \omega_k} \int \frac{d^2 q}{(2\pi)^2} \frac{(\mathbf{e}_k \mathbf{e}_q)^2}{\omega^2 - \omega_q^2 + i0}, \quad (22)$$

where v_0 is the unit cell area. To derive spectrum correction one should put $\omega = \omega_k$ from Eq. (13) and integrate

$$\begin{aligned} \int \frac{d^2 q}{(2\pi)^2} \frac{(\mathbf{e}_k \mathbf{e}_q)^2}{k^2 - q^2 + i0} &= \frac{1}{4\pi} \int_0^{k_D} \frac{q dq}{k^2 - q^2 + i0} \\ &\approx \frac{1}{8\pi} \left(\ln \frac{k^2}{k_D^2 - k^2} - i\pi \right). \end{aligned} \quad (23)$$

Thus the self-energy reads:

$$\Sigma_\gamma^{(2)}(\omega_k, \mathbf{k}) = \frac{\langle \tilde{\gamma}_i^2 \rangle v_0}{16\pi m^2 \tilde{c}^2 \omega_k} \left(\ln \frac{k^2}{k_D^2 - k^2} - i\pi \right). \quad (24)$$

Renormalized spectrum can be found from the following equation:

$$\frac{1}{D(\omega, \mathbf{k})} = \frac{1}{D_0(\omega, \mathbf{k})} - \Sigma^{(2)}(\omega_k, \mathbf{k}) = 0, \quad (25)$$

which has the following solution:

$$\Omega_k = \omega_k \sqrt{1 + \frac{\langle \tilde{\gamma}_i^2 \rangle v_0}{8\pi m^2 \tilde{c}^2 \omega_k^2} \left(\ln \frac{k^2}{k_D^2 - k^2} - i\pi \right)}. \quad (26)$$

The logarithmic divergencies of this spectrum show that for large enough graphene sheets of the size $L \gg 0.1$ mm phonons at the bottom and at the top of the band are localized due to the scattering on disorder. But for actual sizes of graphene sheets this is not the case.

Also, there are corrections to phonon spectrum from perturbation (18), which are negligible at small momenta, but can play significant role out of the long long wavelength region. MD analysis shows that the most important correction is the one containing $\tilde{\zeta}_{jl}^2$. The corresponding equation reads:

$$\begin{aligned} \Sigma_\xi^{(2)}(\omega_k, \mathbf{k}) &= \sum_l \frac{32 \langle \tilde{\zeta}_{jl}^2 \rangle v_0 \sin^2 \frac{k_l}{2}}{m^2 \tilde{c}^2 \omega_k} \\ &\times \int \frac{d^2 q}{(2\pi)^2} \frac{((\mathbf{e}_k - (\mathbf{e}_k \cdot \mathbf{e}_l) \mathbf{e}_l) \cdot (\mathbf{e}_q - (\mathbf{e}_q \cdot \mathbf{e}_l) \mathbf{e}_l))^2 \sin^2 \frac{q_l}{2}}{k^2 - q^2 + i0}, \end{aligned} \quad (27)$$

so for the LA phonons self-energy part of the scattering on disorder has the following form:

$$\Sigma_{LA}^{(2)}(\mathbf{k}) = \Sigma_\gamma^{(2)}(\omega_k, \mathbf{k}) + \Sigma_\xi^{(2)}(\omega_k, \mathbf{k}), \quad (28)$$

and the equation for phonon spectrum valid in the whole Brillouin zone reads:

$$\Omega_k = \omega_k \sqrt{1 + 2\Sigma_{LA}^{(2)}(\mathbf{k})/\omega_k}. \quad (29)$$

C. Theory for ZA phonons

For ZA phonons one can see from expression (4) that we have two different perturbation parts. So let us introduce two sets of parameters, which can be calculated from MD simulation:

$$\alpha = \left\langle \frac{\partial^2 U_{sub}}{\partial z^2}(\mathbf{r}_{i0}, z_{i0}) \right\rangle, \quad (30)$$

$$\alpha_i = \frac{\partial^2 U_{sub}}{\partial z^2}(\mathbf{r}_{i0}, z_{i0}) - \alpha, \quad (31)$$

$$\beta = \left\langle \frac{3K}{4R^2} (z_{i0} - z_{j0})^2 \right\rangle, \quad (32)$$

$$\beta_{ij} = \frac{3K}{4R^2} (z_{i0} - z_{j0})^2 - \beta. \quad (33)$$

Obviously $\langle \alpha_i \rangle = \langle \beta_{ij} \rangle = 0$. Regular translationally invariant part of the Hamiltonian has the following form:

$$\mathcal{H}_{ZA}^{(0)} = \sum_i \left[\frac{p_{zi}^2}{2m} + \frac{\alpha z_i^2}{2} + \sum_j \frac{\beta (z_i - z_j)^2}{2} \right]. \quad (34)$$

Comparing this Hamiltonian with the conventional one for suspended graphene one can see that spectrum is the following:

$$\omega_k = \sqrt{\frac{\alpha}{m} + c_{ZA}^2 k^2}, \quad (35)$$

where

$$c_{ZA} = \left(\frac{2\beta}{K} \right)^{1/2} c. \quad (36)$$

As the phonon-phonon interaction is significant in the case of ZA phonons, we consider the anharmonic term in the Hamiltonian,

$$V = U \sum_{i,j} (z_i - z_j)^4, \quad (37)$$

where summation is conducted over all nearest neighbors, and $U = K/8R^2$. In quantized form:

$$\begin{aligned} V &= \frac{3U}{2m^2 N} \sum_{k_1+k_2=k_3+k_4} \frac{b_{k_1}^+ b_{k_2}^+ b_{k_3} b_{k_4}}{\sqrt{\omega_{k_1} \omega_{k_2} \omega_{k_3} \omega_{k_4}}} \\ &\times \sum_\nu (1 - e^{-ik_1\nu}) (1 - e^{-ik_2\nu}) (1 - e^{ik_3\nu}) (1 - e^{ik_4\nu}). \end{aligned} \quad (38)$$

Linear in U correction is given by the diagram in Fig. 1(c) with corresponding equation in Matsubara technique writing:

$$\Sigma_T(\mathbf{k}) = \frac{12Kv_0}{2mR^2\omega_k} \sum_\nu \sin^2 \frac{k_\nu}{2} \int \frac{d^2 q}{(2\pi)^2} \frac{\sin^2 \frac{q_\nu}{2}}{\omega_q} \coth \frac{\omega_q}{2T}. \quad (39)$$

Thus, the spectrum used henceforth is

$$\omega_k^T = \omega_k \sqrt{1 + \frac{2\Sigma_T(\mathbf{k})}{\omega_k}} \quad (40)$$

Perturbation Hamiltonian has the following form:

$$\mathcal{V} = \sum_i \left[\frac{\alpha_i z_i^2}{2} + \sum_j \frac{\beta_{ij} (z_i - z_j)^2}{2} \right], \quad (41)$$

once again we omit anomalous terms and rewrite the perturbation:

$$\begin{aligned} \mathcal{V} &= \frac{1}{2mN} \sum_j \sum_{k_1, k_2} \frac{b_{k_1}^+ b_{k_2}}{\sqrt{\omega_{k_1} \omega_{k_2}}} e^{i(\mathbf{k}_2 - \mathbf{k}_1) \mathbf{R}_j} \left[\alpha_j \right. \\ &\left. + \sum_l \beta_{jl} (1 - e^{-i\mathbf{k}_1(\mathbf{R}_l - \mathbf{R}_j)}) (1 - e^{i\mathbf{k}_2(\mathbf{R}_l - \mathbf{R}_j)}) \right] \end{aligned} \quad (42)$$

At the small momenta $k \ll 1$ the second order spectrum correction is given only by the term with α_j . As in the previous subsection this correction is logarithmically

divergent for long-wavelength phonons. This indicates their localization at $k \ll a/L$, where a_0 is the lattice parameter and L is graphene flake size. Expressions for all corrections of the second order in disorder strength are presented in Appendix A. Based on results of MD simulations presented in Subsec. IIE, we only keep the two main terms producing the highest contributions, which give the following self-energy:

$$\Sigma_{ZA}^{(2)}(\mathbf{k}) = \frac{v_0}{m^2 \omega_k^T} \left(\langle \alpha_i^2 \rangle I_1(k) + 32 \langle \beta_{jl}^2 \rangle \sum_l \sin^2 \frac{k_l}{2} I_{2l}(\mathbf{k}) \right), \quad (43)$$

where

$$I_1(\mathbf{k}) = \frac{1}{2} \int \frac{d^2 q}{(2\pi)^2} \frac{1}{(\omega_k^T)^2 - (\omega_q^T)^2 + i0}, \quad (44)$$

$$I_{2l}(\mathbf{k}) = \int \frac{d^2 q}{(2\pi)^2} \frac{\sin^2 \frac{q_l}{2}}{(\omega_k^T)^2 - (\omega_q^T)^2 + i0}. \quad (45)$$

The corresponding expression for ZA phonon spectrum reads:

$$\Omega_k = \omega_k^T \sqrt{1 + 2 \Sigma_{ZA}^{(2)}(\mathbf{k}) / \omega_k^T}. \quad (46)$$

D. Phonon scattering mechanisms in graphene

The conventional mechanisms of phonon lifetime reduction in graphene are scattering on the graphene flake boundaries and anharmonic three-phonon scattering processes. The contributions to phonon damping associated with boundary scattering can be written as $\tau_L^{-1} = v_k/L$, where $v_k = \frac{\partial \omega_k}{\partial k}$ is the phonon group velocity, L estimates the graphene sample size. For the in-plane phonons the averaged sound velocity can be taken without loss of accuracy. The contribution of anharmonic processes to phonon damping can be described with relation^{31,46}

$$\tau_{anh}^{-1} = (B_N + B_U \exp(-\Theta/BT)) \omega^2 \tau^3, \quad (47)$$

where $\Theta \approx 1000\text{K}$ is the Debye temperature, $B = 3$, $B_N = B_U/2$ and $B_U = 7.7 \cdot 10^{-25} \text{ sK}^{-3}$.

The substrate-induced disorder studied in previous sections also leads to reduction of the phonon lifetime. Corresponding value can be derived as a reciprocal imaginary part of phonon spectrum given by (29) and (46) for in-plane and flexural phonons, respectively: $\tau_{substr}^{-1} = \Im\{\Omega_k\}$. The total lifetime is given by Matthiessen's rule $\tau_{total}^{-1} = \tau_L^{-1} + \tau_{anh}^{-1} + \tau_{substr}^{-1}$.

The contribution to heat conductivity of graphene from a given phonon mode obtained on the basis of Boltzmann transport equation within the relaxation time approximation can be written as

$$\kappa = \frac{\hbar}{h} \int k dk \tau_{total}(k) \omega_k \frac{\partial N^0(\omega_k)}{\partial T} v_k^2, \quad (48)$$

where $N^{(0)}$ is equilibrium Bose distribution function and h is the graphene layer thickness.

E. Molecular dynamics simulation

The GROMACS⁴⁷ package was used to perform all MD simulations. The $72\text{\AA} \times 72\text{\AA} \times 36\text{\AA}$ amorphous SiO_2 substrate consisting of 12000 atoms was rigid. The round graphene sheet of diameter $D \approx 40\text{\AA}$ consisted of 481 carbon atoms. The C-C interactions within the graphene sheet were modeled with harmonic potential $K = 27 \text{ eV/\AA}^2$, which corresponds to the first neighbor interatomic force constant from⁴⁸. This model is consistent with employed analytical description of graphene vibrational properties. Interactions between C atoms of graphene and Si and O atoms of the substrate were modeled with Lennard-Jones potential with parameters taken from⁴³.

Graphene sheet initial position was 1\AA above the substrate. Simulation was performed with 0.02 ps timestep, the temperature was controlled with weak coupling algorithm⁴⁹. During the first 500 ps graphene sheet was attracted by the substrate and started planar diffusion on its surface. Then from initial value of 300 K temperature was lowered to zero for 500 ps using velocity rescale temperature coupling⁴⁹. The obtained frozen equilibrium configuration of graphene on SiO_2 substrate was treated in Mathematica⁵⁰ package to derive the parameters required by the theory. Only carbon atoms with three neighbors were considered. The results exhibit no significant dependence on initial conditions of MD simulations. The required by perturbation theory graphene-substrate interaction energetic parameters are listed in the Table. Fig. 2 shows the obtained geometry of graphene on the amorphous SiO_2 substrate.

The atomic Z coordinate root mean square displacement for graphene on the substrate with respect to initial unperturbed graphene is 0.04 nm . For the X and Y coordinates we obtain 0.007 nm . This is closely related with the fact that contribution of the term with r_{i0}^τ in ξ_{ij} (see Eq. (8)) is much less than one with z_{i0} and in the definition of β_{ij} (32) it can be completely omitted. With high accuracy $\beta = 3\xi$ and $\sqrt{\langle \beta_{ij}^2 \rangle} = 3\sqrt{\langle \xi_{jl}^2 \rangle}$.

III. RESULTS AND DISCUSSION

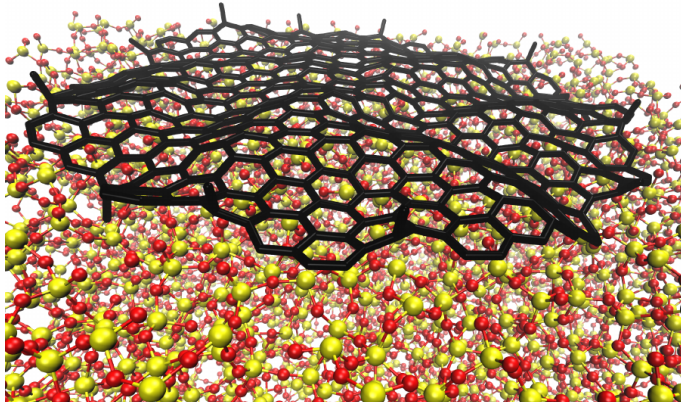
A. Spectra and relaxation times of in-plane phonons

Substrate influence on the in-plane phonons in graphene constitutes in the following effects. First, according to Eq. (13) interaction with substrate leads to the opening of band gap of approx. 22 K , see Fig. 3. It results the phonon occupation number suppression for low temperatures and corresponding reduction of graphene thermal conductivity for temperatures lower than 20 K .

Secondly, the scattering by the substrate-induced disorder leads to extra reduction of phonon lifetime. Fig.

TABLE I. The obtained with MD parameters required by perturbation theory. All values are given in eV/Å²

In-plane phonons				ZA phonons			
γ	$\sqrt{\langle \tilde{\gamma}_i^2 \rangle}$	ξ	$\sqrt{\langle \xi_{jt}^2 \rangle}$	α	$\sqrt{\langle \alpha_i^2 \rangle}$	β	$\sqrt{\langle \beta_{ij}^2 \rangle}$
0.006	0.015	0.2	0.28	0.09	0.11	0.59	0.82

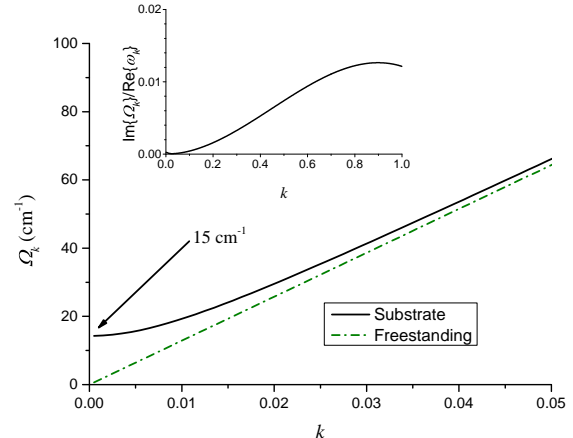
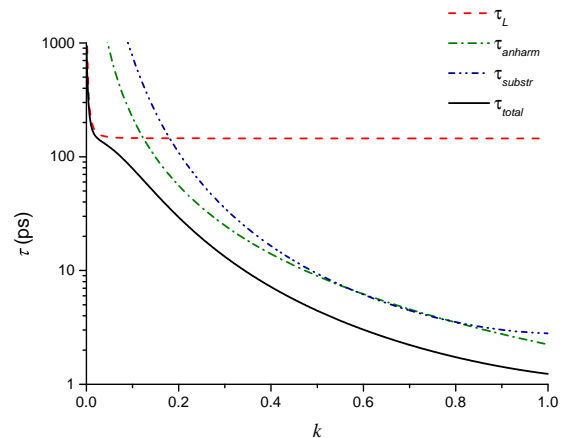
FIG. 2. Color online. Final structure of graphene on amorphous SiO₂ obtained with MD simulation.

4 shows the dependence of the relaxation time on the phonon wave vector magnitude for various mechanisms. We take graphene sample size $L = 2.9 \mu\text{m}$. Phonon lifetime for anharmonic processes is given for 300K. One sees that at low temperatures long wavelength phonons give the main contribution to the heat conductivity. In both suspended (freestanding) and supported graphene the boundary scattering is the dominant mechanism of phonon damping. For shorter wavelength phonons excited at temperatures from 100K to 300K the dominant mechanism corresponds to substrate-induced disorder scattering in graphene on amorphous SiO₂ and to anharmonic processes. For higher temperatures, the anharmonic processes become dominant for both supported and freestanding graphene.

B. Spectra and relaxation times of ZA phonons

It is clear that the bare phonon spectrum given by Eq. (35) significantly differs from quadratic spectrum of freestanding graphene, given by $\omega_k = Ak^2$, where $A = 3.13 \cdot 10^{-3} \text{cm}^2\text{s}^{-151}$. The phonon-phonon interaction described by (40) leads to the effective increasing of c_{ZA} . For $T = 300 \text{K}$ the value of c_{ZA} is 6 km/s or approximately 30% of the in-plane phonon velocity. We predict that the spectrum of such form will be actual for graphene on substrates with low disorder, i.e. crystalline Si or Diamond.

Fig. 5(a) shows the real and the imaginary parts of ZA phonon spectrum for $T = 300\text{K}$ calculated with Eq. (46) using parameters from Table I and Fig. 5(b) shows

FIG. 3. Color online. Dispersion relations of in-plane acoustic phonons in freestanding graphene and in graphene on substrate. The inset shows the spectrum imaginary to real ratio for graphene on disordered substrate. Phonon wave vector k is given in units of π/a_0 and $k = 1$ corresponds to the boundary of the Brillouin zone.FIG. 4. Color online. Acoustic in-plane phonons relaxation times corresponding to various mechanisms of scattering. Red dashed curve is for relaxation time related to boundary scattering τ_L with $L = 2.9 \mu\text{m}$. Green dash-dot curve is for anharmonic processes for temperature $T=300 \text{K}$. Blue dash-dot-dot curve is for substrate-induced phonon damping. Black curve is total phonon lifetime, derived with Matthiessen's rule.

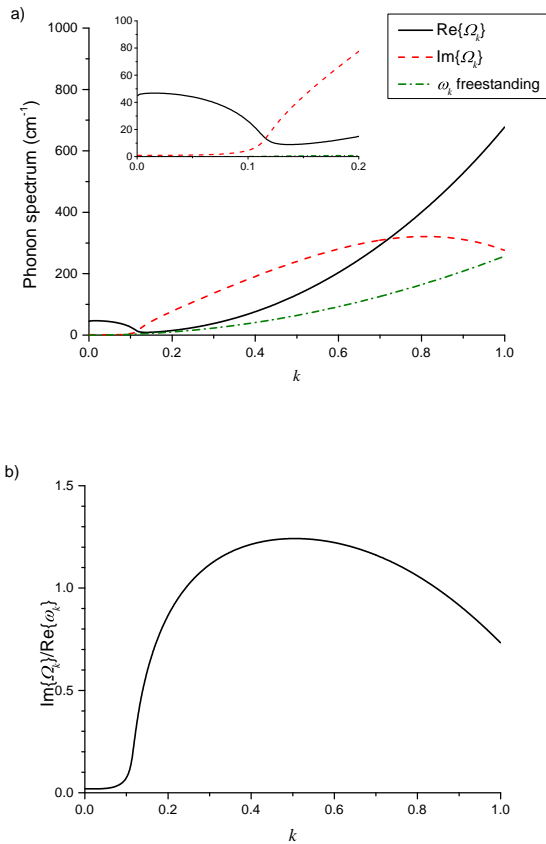


FIG. 5. Color online. a) Calculated spectrum of ZA phonons in graphene on amorphous substrate. Solid black curve and red dashed curve are for real and imaginary parts of ZA phonon spectrum at $T = 300$ K for graphene on amorphous substrate, respectively. Green dash dot curve is for ZA phonon spectrum of freestanding graphene. b) Ratio of imaginary part of ZA phonon spectra to real part of bare spectra for graphene on disordered substrate.

the ZA phonon spectrum imaginary to real part ratio.

In the considered system we have strong disorder for ZA phonons with spectrum ω_k^T calculated via Eq. (40). It is well known that even disorder with small concentration leads to localization of long-wavelength excitations (for bosonic systems see E.G. Refs.⁵²⁻⁵⁴). But here "impurities concentration" is equal to 1, providing spectrum corrections of the order of the pure spectrum (40) in the whole Brillouin zone (see Fig. 5(a)), which makes ZA phonons overdamped (see Fig. 5(b)) and their nature is a question of further considerations, the possible scenario is localization of all ZA phonon modes. Anyway, from our theory it is quite natural to make a conclusion that ZA phonons do not contribute to graphene on amorphous substrate heat conductivity.

Even if the thermal conductivity of such ZA phonons graphene is calculated using the BTE, where one assumes $v_k = \frac{\partial}{\partial k} \Re\{\Omega_k\}$ and $\tau_{substr}^{-1} = \Im\{\Omega_k\}$, it is lower than $20 \text{ Wm}^{-1}\text{K}^{-1}$ and should be neglected in compari-

son with the contribution of the in-plane phonons. This can be explained by significant reduction of the phonon mean lifetime due to scattering by the substrate. Fig. 5(a) with the characteristic magnitude of ZA phonon spectrum imaginary part shows that τ_{substr} is lower than 0.1 ps in most volume of Brillouin zone.

C. Graphene heat conductivity

Fig. 6 shows the experimentally measured heat conductivity of freestanding and supported graphene and corresponding theoretical predictions based on the developed perturbation theory and BTE.

As mentioned above, the graphene-substrate interaction suppresses the contribution of ZA phonons to heat conductivity in the whole range of temperatures for graphene bonded with amorphous SiO_2 substrate. This contribution is negligible due to ZA phonon localization and extremely short lifetime. Therefore, the total heat conductivity is governed by in-plane phonons.

For temperatures below 100 K the in-plane phonon heat conductivity is governed by boundary scattering for both supported and suspended graphene. For temperatures above 300 K the dominant mechanism corresponds to the anharmonic processes. Our theory shows that in-plane phonon heat conductivity is not affected strongly by the substrate. Taking into account vanishing ZA phonon contribution, heat conductivity is approximately two times smaller.

Between 100 K and 300 K both the contributions of the substrate and anharmonic processes are comparable. Interplay between the characteristic lifetimes for substrate disorder-induced scattering and anharmonic processes defines the values of heat conductivity. As a result it is several times smaller than for freestanding graphene, which is in a good agreement with available experimental data.

Experimental data from Ref.²⁸ indicate significant suppression of the supported graphene heat conductivity below 300 K and shifting the maximum from approx. 200 K for freestanding graphene to 300 K. At low temperatures only long wavelength phonons are excited and give contribution to heat conductivity. We thus conclude that the long wavelength phonon lifetime is reduced by the substrate. To bring the developed theory in agreement with the experimentally confirmed long wavelength phonons lifetime reduction, the assumption $L = 0.2 \mu\text{m}$ was made, whereas the experiment yields graphene sheet size of the order of micron. This discrepancy may be due to the long-range disorder correlations, which are not taken into account in present theory. Alternatively, to explain the observed experimental behavior of heat conductivity, the authors of Ref.²⁸ develop a theory, which is based on the Fermi golden rule and apply Klemens formalism³⁶ to the case of a large area spot contact between graphene and substrate. In their model, the suppression of long wavelength phonon lifetime stems from an arguable as-

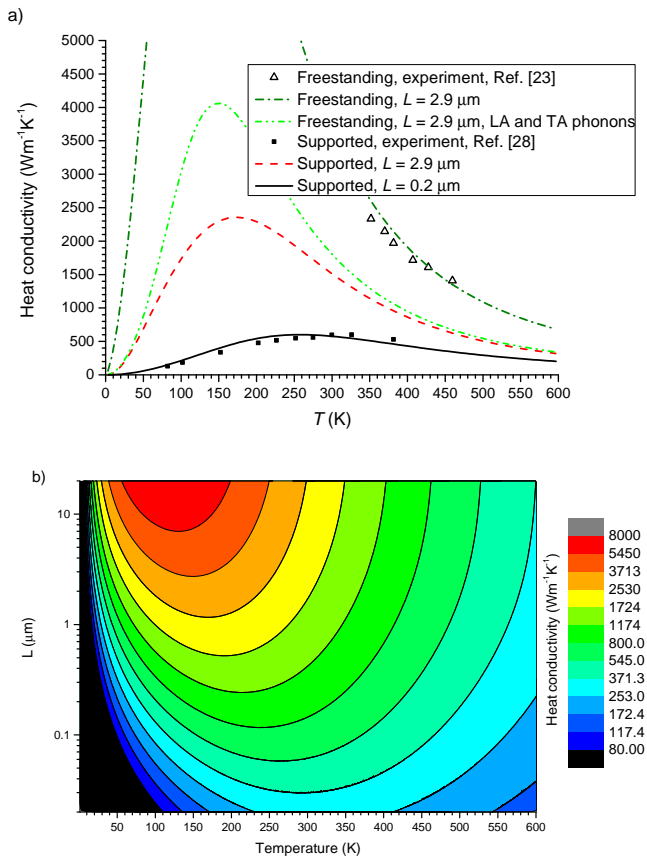


FIG. 6. Color online. Panel a). Heat conductivity of freestanding graphene, obtained by Raman optothermal method (open triangles)²³ and calculated by BTE as a sum of in-plane and ZA phonons contributions (dark green dash-dot curve). Graphene flake size $L = 2.9 \mu\text{m}$. Contribution of in-plane phonons to heat conductivity of freestanding graphene is presented separately with light green dash-dot-dot curve. Total heat conductivity of graphene on amorphous substrate given by in-plane phonons only is denoted by red dashed curve. ZA contribution is absent, only in-plane phonons play a role, graphene size is the same: $L = 2.9 \mu\text{m}$. Black solid squares denote the experimental data for the supported graphene²⁸. Black solid curve is for heat conductivity of graphene on amorphous substrate and $L = 0.2 \mu\text{m}$. Panel b). The obtained within the developed theory dependence of supported graphene heat conductivity on temperature T and size L .

sumption of a constant phonon scattering matrix element. The conventional form of matrix element given in³⁶ is quadratic in the phonon frequency, which yields suppression of high frequency phonons instead, see Eq. (32) in Ref.³⁴.

It is also necessary to compare the obtained data on the phonon lifetimes and graphene thermal conductivity with results of the MD simulations. Fig. 2 from Ref.⁴³ shows that the lifetime of both in-plane and ZA phonons in suspended graphene lies in the range from 10 to 25 ps. For supported graphene, the characteristic lifetimes of all phonon modes are from several picoseconds to 10 ps.

These results are in contradiction with the relatively weak effect of the substrate on the in-plane phonons and dramatic suppression of the ZA phonon lifetime predicted here. Other studies lie in agreement with our predictions. MD simulations performed in Ref.⁴⁴ yield 90% reduction of ZA phonon contribution to the thermal conductivity and spectrum deformation for actual strength of the graphene-substrate interaction, which coincides with the results of the present study. Finally, Ref.³⁹ predicts localization of excitations in amorphous graphene and corresponding two-fold decrease of heat conductivity.

The predictions on graphene heat conductivity are robust with respect to variation of the energetic parameters from the Table I. Although we account only pair harmonic potential for C-C bonds in MD simulations, we argue that using more sophisticated model (E.G. accounting for three-particle torsional rigidity and next neighbors interactions) would slightly renormalize the parameters and the obtained qualitative picture remains intact.

The employed model lies in agreement with the fact that graphene sheets conform to the underlying silicon oxide substrate, reported in^{55,56}. However, this model does not account for long-range (20 nm) height correlations of the substrate and graphene. Also these studies report that graphene sheet conforms the substrate corrugations but with smaller amplitude, which is an evidence of graphene being partially suspended. The elucidation of the geometry of graphene interacting via van der Waals force with amorphous substrates is to be clarified in further experimental studies and MD simulations. The developed model is rather related to the atomically smooth substrates. The considered effect of amorphous substrate on graphene intrinsic heat conductivity is important when creating graphene-based electronic devices with the heat-sink functions placed on graphene pathways and should be taken into account when managing circuit thermal parameters.

ACKNOWLEDGMENTS

Sergei Koniakhin acknowledges support by the Russian Science Foundation (Project No. 16-19-00075 Thermo-electric generator with record parameters based on carbon nanostructures: development of scientific bases”). Oleg Utiosov acknowledges Russian Science Foundation (Project No 14-22-00281 “Low dimensional quantum field theory in elementary particles and condensed matter physics”). This work was partly supported by the Skolkovo Foundation (Grant agreement for Russian educational and scientific organization no. 4dd.25.12.2014 to Ivan Terterov). Anton Nalitov acknowledges financial support from the EPSRC Established Career fellowship of A.V. Kavokin. The authors are grateful to M.V. Dubina for his attention to the work, to A.V. Syromyatnikov and A.G. Yashenkin for valuable discussions and to E.D. Eidelman for his support.

Appendix A: ZA phonons self-energy part corrections

From (41) we see that in the second order in disorder strength we have different corrections. We treat this perturbation conventionally, considering only the terms with disorder constants corresponds to the same site. Thus, we have four terms, proportional to $\langle \alpha_i^2 \rangle$, $\langle \beta_{ij}^2 \rangle$, $\langle \alpha_i \beta_{ij} \rangle$ and $\langle \beta_{jl} \beta_{jm} \rangle$ for $l \neq m$.

Correction proportional to $\langle \alpha_i^2 \rangle$ is logarithmically divergent at very small momenta k and contains the following integral

$$I_1(k) = \frac{1}{2} \int \frac{d^2 q}{(2\pi)^2} \frac{1}{(\omega_k^T)^2 - (\omega_q^T)^2 + i0} \quad (\text{A1})$$

The second correction stems from nonzero average $\langle \beta_{ij}^2 \rangle$. Corresponding equation is

$$\sum_l \frac{32 \langle \beta_{jl}^2 \rangle v_0 \sin^2 \frac{k_l}{2}}{m^2 \omega_k^T} \int \frac{d^2 q}{(2\pi)^2} \frac{\sin^2 \frac{q_l}{2}}{(\omega_k^T)^2 - (\omega_q^T)^2 + i0}, \quad (\text{A2})$$

where summation is over three possible neighbors positions and q_l and k_l are corresponding momenta projections. We denote corresponding integral as

$$I_{2l}(k) = \int \frac{d^2 q}{(2\pi)^2} \frac{\sin^2 \frac{q_l}{2}}{(\omega_k^T)^2 - (\omega_q^T)^2 + i0}. \quad (\text{A3})$$

The third correction is due to correlations between α_i and β_{ij} . Corresponding equation is

$$\frac{2v_0 \langle \alpha_i \beta_{il} \rangle}{m^2 \omega_k^T} \sum_l \int \frac{d^2 q}{(2\pi)^2} \frac{f(\mathbf{k}, \mathbf{q}, l)}{(\omega_k^T)^2 - (\omega_q^T)^2 + i0}, \quad (\text{A4})$$

where

$$f(\mathbf{k}, \mathbf{q}, l) = 1 + \cos(k_l - q_l) - \cos k_l - \cos q_l. \quad (\text{A5})$$

Expression (A4) can be simplified using

$$1 + \cos(k_l - q_l) - \cos k_l - \cos q_l = \sin k_l \sin q_l + 4 \sin^2 \frac{k_l}{2} \sin^2 \frac{q_l}{2}, \quad (\text{A6})$$

the first term gives zero after integration over angle, so the correction obeys following form

$$\frac{8v_0 \langle \alpha_i \beta_{il} \rangle}{m^2 \omega_k^T} \sum_l \sin^2 \frac{k_l}{2} \int \frac{d^2 q}{(2\pi)^2} \frac{\sin^2 \frac{q_l}{2}}{(\omega_k^T)^2 - (\omega_q^T)^2 + i0}, \quad (\text{A7})$$

corresponding integral denotation is

$$I_{3l}(k) = \int \frac{d^2 q}{(2\pi)^2} \frac{\sin^2 \frac{q_l}{2}}{(\omega_k^T)^2 - (\omega_q^T)^2 + i0}. \quad (\text{A8})$$

The last correction arises from correlations between β_{ij} and β_{il} , where j and l denote different neighboring sites. Corresponding equation is

$$\sum_{l \neq m} \frac{32 \langle \beta_{jl} \beta_{jm} \rangle v_0}{m^2 \omega_k^T} \int \frac{d^2 q}{(2\pi)^2} \frac{g(\mathbf{k}, \mathbf{q}, l, m)}{(\omega_k^T)^2 - (\omega_q^T)^2 + i0}, \quad (\text{A9})$$

where

$$g(\mathbf{k}, \mathbf{q}, l, m) = \cos \frac{(\mathbf{k} - \mathbf{q})(\mathbf{e}_m - \mathbf{e}_l)}{2} \times \sin \frac{k_l}{2} \sin \frac{k_m}{2} \sin \frac{q_l}{2} \sin \frac{q_m}{2}, \quad (\text{A10})$$

so

$$I_{4lm}(k) = \int \frac{d^2 q}{(2\pi)^2} \frac{g(\mathbf{k}, \mathbf{q}, l, m)}{(\omega_k^T)^2 - (\omega_q^T)^2 + i0}. \quad (\text{A11})$$

Real parts of this expressions are the principal values of corresponding integrals, and imaginary parts are

$$\Im \left[\int \frac{d^2 q}{(2\pi)^2} \frac{F(\mathbf{k}, \mathbf{q})}{k^2 - q^2 + i0} \right] = - \frac{\pi}{(2\pi)^2} \int d\varphi \frac{k F(\mathbf{e}_k, \mathbf{e}_q, q = k)}{\frac{\partial (\omega_q^T)^2}{\partial q}(k)} \quad (\text{A12})$$

The obtained with MD simulations values of energetic parameters are $\sqrt{\langle \alpha_i \beta_{ij} \rangle} = \sqrt{-0.016 \text{ eV/\AA}^2}$ and $\sqrt{\langle \beta_{ij} \beta_{ik} \rangle} = \sqrt{-0.002 \text{ eV/\AA}^2}$.

Appendix B: Approximation of integral in the in-plane phonon self-energy part correction

The integral in Eq. (27) required for calculating $\Sigma_\xi^{(2)}$ and τ_{substr} for in-plane phonons can be approximated with sufficient accuracy as follows:

$$\sum_l \sin^2 \frac{k_l}{2} \times \int \frac{d^2 q}{(2\pi)^2} \frac{((\mathbf{e}_k - (\mathbf{e}_k \cdot \mathbf{e}_l)\mathbf{e}_l) \cdot (\mathbf{e}_q - (\mathbf{e}_q \cdot \mathbf{e}_l)\mathbf{e}_l))^2 \sin^2 \frac{q_l}{2}}{k^2 - q^2 + i0} \approx 0.2k^2 - 2.2k^3 + 2.33k^4 - i(1.51k^4 - 1.11k^5). \quad (\text{B1})$$

Its dependence on the direction of \mathbf{k} with respect to graphene bonds is weak.

* kon@mail.ioffe.ru

† utiosov@gmail.com

- ¹ I. Frank, D. M. Tanenbaum, A. Van der Zande, and P. L. McEuen, *Journal of Vacuum Science & Technology B* **25**, 2558 (2007).
- ² C. Lee, X. Wei, J. W. Kysar, and J. Hone, *science* **321**, 385 (2008).
- ³ A. H. Castro Neto, F. Guinea, N. M. R. Peres, K. S. Novoselov, and A. K. Geim, *Rev. Mod. Phys.* **81**, 109 (2009).
- ⁴ S. Das Sarma, S. Adam, E. H. Hwang, and E. Rossi, *Rev. Mod. Phys.* **83**, 407 (2011).
- ⁵ E. H. Hwang, S. Adam, and S. Das Sarma, *Phys. Rev. Lett.* **98**, 186806 (2007).
- ⁶ A. V. Nalitov, L. E. Golub, and E. L. Ivchenko, *Phys. Rev. B* **86**, 115301 (2012).
- ⁷ M. Glazov and S. Ganichev, *Physics Reports* **535**, 101 (2014), high frequency electric field induced nonlinear effects in graphene.
- ⁸ J. Karch, C. Drexler, P. Olbrich, M. Fehrenbacher, M. Hirmer, M. M. Glazov, S. A. Tarasenko, E. L. Ivchenko, B. Birkner, J. Eroms, D. Weiss, R. Yakimova, S. Lara-Avila, S. Kubatkin, M. Ostler, T. Seyller, and S. D. Ganichev, *Phys. Rev. Lett.* **107**, 276601 (2011).
- ⁹ P. Dollfus, V. H. Nguyen, *et al.*, *Journal of Physics: Condensed Matter* **27**, 133204 (2015).
- ¹⁰ A. A. Balandin, *Nature materials* **10**, 569 (2011).
- ¹¹ D. L. Nika and A. A. Balandin, *Journal of Physics: Condensed Matter* **24**, 233203 (2012).
- ¹² T. Ando, *Journal of the Physical Society of Japan* **75**, 074716 (2006), <http://dx.doi.org/10.1143/JPSJ.75.074716>.
- ¹³ M. Ishigami, J. H. Chen, W. G. Cullen, M. S. Fuhrer, and E. D. Williams, *Nano Letters* **7**, 1643 (2007), pMID: 17497819, <http://dx.doi.org/10.1021/nl070613a>.
- ¹⁴ S. V. Morozov, K. S. Novoselov, M. I. Katsnelson, F. Schedin, D. C. Elias, J. A. Jaszczak, and A. K. Geim, *Phys. Rev. Lett.* **100**, 016602 (2008).
- ¹⁵ M. Katsnelson and A. Geim, *Philosophical Transactions of the Royal Society of London A: Mathematical, Physical and Engineering Sciences* **366**, 195 (2008), <http://rsta.royalsocietypublishing.org/content/366/1863/195.full.pdf>.
- ¹⁶ H. Sevinli and M. Brandbyge, .
- ¹⁷ J.-H. Chen, C. Jang, S. Xiao, M. Ishigami, and M. S. Fuhrer, *Nat Nano* **3**, 206 (2008).
- ¹⁸ S. Fratini and F. Guinea, *Phys. Rev. B* **77**, 195415 (2008).
- ¹⁹ V. Perebeinos and P. Avouris, *Phys. Rev. B* **81**, 195442 (2010).
- ²⁰ S. S. Kubakaddi and K. S. Bhargavi, *Phys. Rev. B* **82**, 155410 (2010).
- ²¹ S. Koniakhin and E. Eidelman, *EPL (Europhysics Letters)* **103**, 37006 (2013).
- ²² W. Cai, A. L. Moore, Y. Zhu, X. Li, S. Chen, L. Shi, and R. S. Ruoff, *Nano letters* **10**, 1645 (2010).
- ²³ S. Chen, A. L. Moore, W. Cai, J. W. Suk, J. An, C. Mishra, C. Amos, C. W. Magnuson, J. Kang, L. Shi, *et al.*, *ACS nano* **5**, 321 (2010).
- ²⁴ S. Ghosh, I. Calizo, D. Teweldebrhan, E. Pokatilov, D. Nika, A. Balandin, W. Bao, F. Miao, and C. N. Lau, *Applied Physics Letters* **92**, 151911 (2008).
- ²⁵ A. A. Balandin, S. Ghosh, W. Bao, I. Calizo, D. Teweldebrhan, F. Miao, and C. N. Lau, *Nano letters* **8**, 902 (2008).
- ²⁶ C. Faugeras, B. Faugeras, M. Orlita, M. Potemski, R. R. Nair, and A. Geim, *ACS nano* **4**, 1889 (2010).
- ²⁷ S. Chen, Q. Wu, C. Mishra, J. Kang, H. Zhang, K. Cho, W. Cai, A. A. Balandin, and R. S. Ruoff, *Nature materials* **11**, 203 (2012).
- ²⁸ J. H. Seol, I. Jo, A. L. Moore, L. Lindsay, Z. H. Aitken, M. T. Pettes, X. Li, Z. Yao, R. Huang, D. Broido, *et al.*, *Science* **328**, 213 (2010).
- ²⁹ R. Murali, Y. Yang, K. Brenner, T. Beck, and J. D. Meindl, *Applied Physics Letters* **94**, 243114 (2009).
- ³⁰ A. D. Liao, J. Z. Wu, X. Wang, K. Tahy, D. Jena, H. Dai, and E. Pop, *Physical review letters* **106**, 256801 (2011).
- ³¹ A. Alofi and G. P. Srivastava, *Journal of Applied Physics* **112**, 013517 (2012).
- ³² D. Nika, E. Pokatilov, A. Askerov, and A. Balandin, *Physical Review B* **79**, 155413 (2009).
- ³³ D. Nika, S. Ghosh, E. Pokatilov, and A. Balandin, *Applied Physics Letters* **94**, 203103 (2009).
- ³⁴ P. Klemens and D. Pedraza, *Carbon* **32**, 735 (1994).
- ³⁵ L. Lindsay, D. A. Broido, and N. Mingo, *Phys. Rev. B* **82**, 115427 (2010).
- ³⁶ P. Klemens, *Proceedings of the Physical Society. Section A* **68**, 1113 (1955).
- ³⁷ H. Zhang, G. Lee, and K. Cho, *Physical Review B* **84**, 115460 (2011).
- ³⁸ Z. Wei, Z. Ni, K. Bi, M. Chen, and Y. Chen, *Carbon* **49**, 2653 (2011).
- ³⁹ T. Zhu and E. Ertekin, *Nano Letters* (2016).
- ⁴⁰ T. Zhu and E. Ertekin, *Phys. Rev. B* **90**, 195209 (2014).
- ⁴¹ Z.-Y. Ong, E. Pop, and J. Shiomi, *Phys. Rev. B* **84**, 165418 (2011).
- ⁴² D. Donadio and G. Galli, *Phys. Rev. Lett.* **99**, 255502 (2007).
- ⁴³ B. Qiu and X. Ruan, *Applied Physics Letters* **100**, 193101 (2012), <http://dx.doi.org/10.1063/1.4712041>.
- ⁴⁴ Z.-Y. Ong and E. Pop, *Physical Review B* **84**, 075471 (2011).
- ⁴⁵ A. Göbel, D. Wang, M. Cardona, L. Pintschovius, W. Reichardt, J. Kulda, N. Pyka, K. Itoh, and E. Haller, *Physical Review B* **58**, 10510 (1998).
- ⁴⁶ G. P. Srivastava, *The physics of phonons* (CRC Press, 1990).
- ⁴⁷ B. Hess, C. Kutzner, D. van der Spoel, and E. Lindahl, *Journal of Chemical Theory and Computation* **4**, 435 (2008), <http://pubs.acs.org/doi/pdf/10.1021/ct700301q>.
- ⁴⁸ O. Dubay and G. Kresse, *Phys. Rev. B* **67**, 035401 (2003).
- ⁴⁹ G. Bussi, D. Donadio, and M. Parrinello, *The Journal of chemical physics* **126**, 014101 (2007).
- ⁵⁰ W. Research, “Mathematica 8.0,” (2010).
- ⁵¹ T. Nihira and T. Iwata, *Phys. Rev. B* **68**, 134305 (2003).
- ⁵² A. Chaudhuri, A. Kundu, D. Roy, A. Dhar, J. L. Lebowitz, and H. Spohn, *Phys. Rev. B* **81**, 064301 (2010).
- ⁵³ M. N. Luckyanova, J. Mendoza, H. Lu, S. Huang, J. Zhou, M. Li, B. J. Kirby, A. J. Grutter, A. A. Puzosky, M. S. Dresselhaus, *et al.*, arXiv preprint arXiv:1602.05057 (2016).
- ⁵⁴ O. I. Utesov, A. V. Sizanov, and A. V. Syromyatnikov, *Phys. Rev. B* **90**, 155121 (2014).
- ⁵⁵ M. Ishigami, J. Chen, W. Cullen, M. Fuhrer, and E. Williams, *Nano letters* **7**, 1643 (2007).
- ⁵⁶ V. Geringer, M. Liebmann, T. Echtermeyer, S. Runte, M. Schmidt, R. Rückamp, M. C. Lemme, and M. Morgenstern, *Physical review letters* **102**, 076102 (2009).